Numerical Study on the Concrete Microstructure using Image-based Virtual Element Method

Hyeong-Tae Kim, PhD

Kyoungsoo Partk, PhD

May 31, 2023

Computational & Experimental Mechanics Group
School of Civil & Environmental Engineering
Yonsei University, Seoul, Korea

Motivation

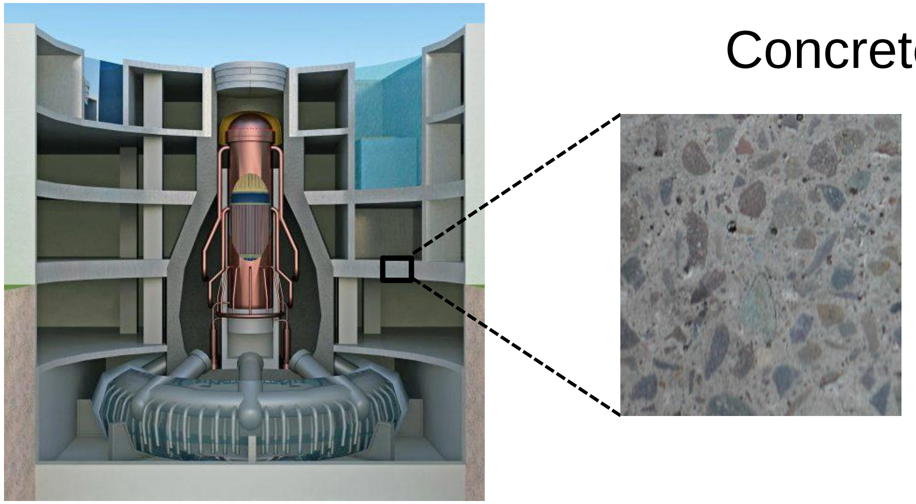

Concrete Microstructure Analysis

- Complexity of microstructure
- Wide range of length scale

Discretization of complex-geometry mesh
Number of elements increase

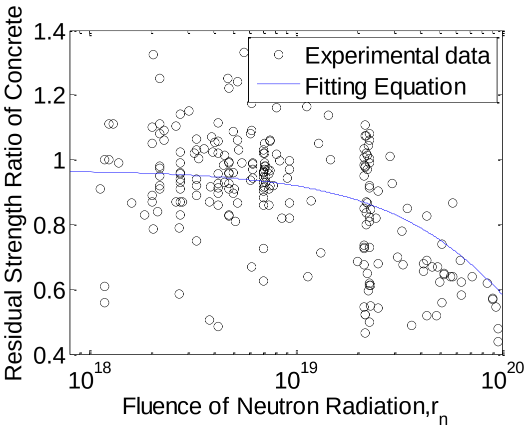

Virtual Element Method

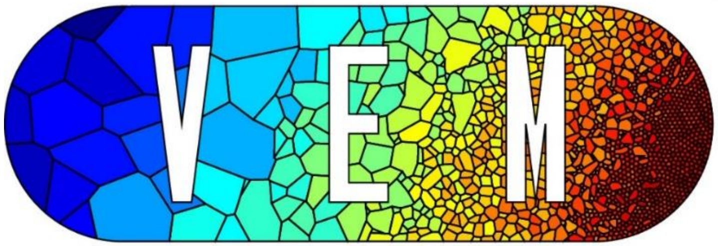

- K. Park, H.T. Kim, T.H. Kwon, and E. Choi, 2016, *Nuclear Engineering and Design* 310, 15-26
- Pignatelli, I., Kumar, A., Field, K.G., Wang, B., Yu, Y., Le Pape, Y., Bauchy, M. and Sant, G., 2016. *Scientific Reports*, 6, 20155
- Maruyama, I., Kontani, O., Takizawa, M., Sawada, S., Ishikawao, S., Yasukouchi, J., … Igari, T. 2017. *Journal of Advanced Concrete Technology*, 15(9), 440–523.
- Choi, H., Chi, H., Park, K., & Paulino, G. H. 2021. *International Journal of Numerical Methods in Engineering, 122*(1), 25-52

Contents

- **Motivation**
- **Image Based Analysis**
  - Microstructure Reconstruction
  - Mesh Generation based on the Image
- **Numerical Analysis**
  - Virtual Element Formulation
  - Uniaxial Tension Test
  - Aggregate Volume Expansion
- **Summary**

Image Preparation

◻ Concrete Specimen

Mix component		Content (kg/m^3)	Volume (m^3)
Portland Cement		425	137.1
Water		166	166.0
Aggregate	Quartz sand [석영] 0-2 mm	525	198.1
	Gabbro [반려암] 2-8 mm	1267	448.0
Admixture	Plasticizer	2.89	2.8
	Air entraining agent	0.77	0.7

◻ Computed Tomography

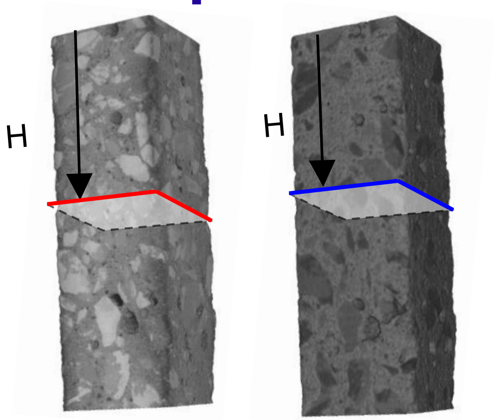

Specimen size = 20 x 20 x 80 mm

X-ray CT pixel size ≈ 13.8 μm

Neutron CT pixel size ≈ 43.0 μm

V. Szilágyi, K. Gméling, Z. Kis, I. Harsányi, L. Szentmiklósi (2019). Neutron-based methods for the development of concrete. Proceedings of the 12th International Symposium on Brittle Matrix Composites, BMC 2019, 183-193

D.F.T. Razakamandimby, & K, Park. (2019). Characterization of air entrained concrete porosity using X-ray computed micro tomography image analysis. Proceedings of the 12th International Symposium on Brittle Matrix Composites, BMC 2019, 139-146

Image Segmentation

◻ X-ray CT (Depend on the material density)

Image Segmentation : Otsu method

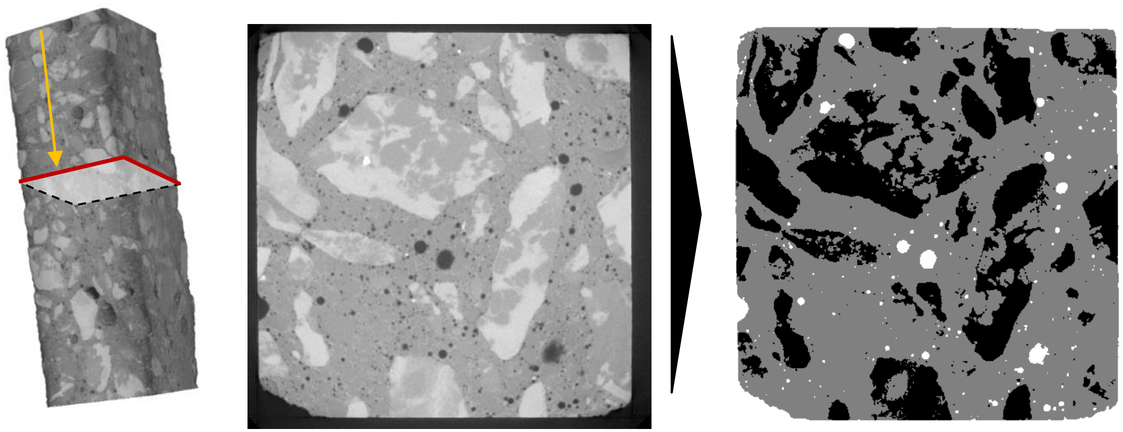

$\rho_{Quartz} = 2.67$ g/cm^3
(Howie et al. 1992)

$\rho_{C-S-H} = 2.604$ g/cm^3
(Allen et al. 2007)

◻ Neutron CT (Depend on the hydrogen component)

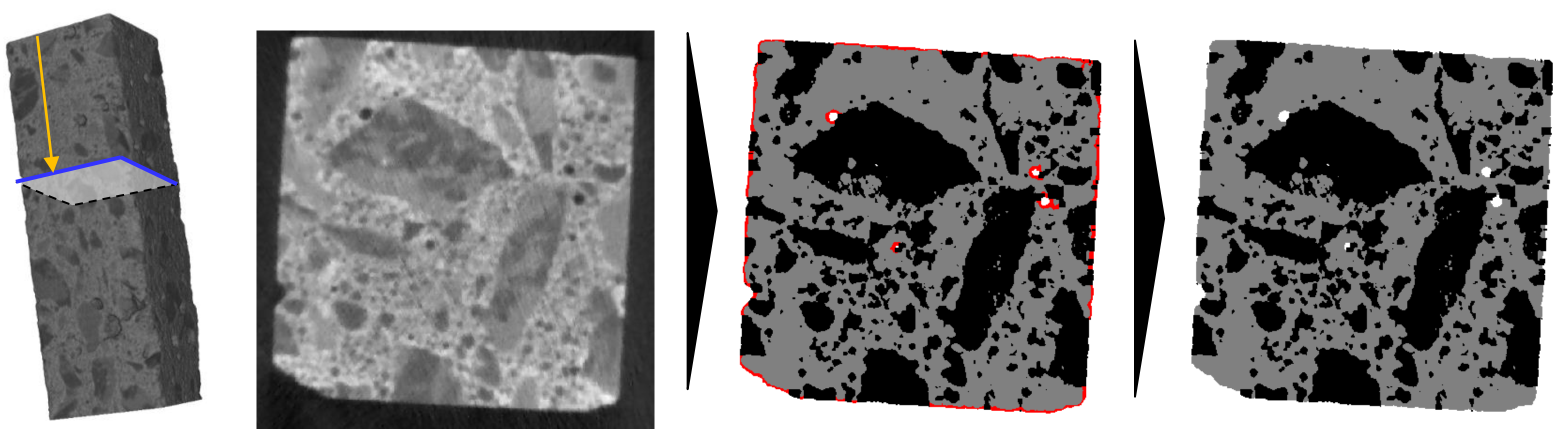

Remove partial volume effect

Microstructure Reconstruction

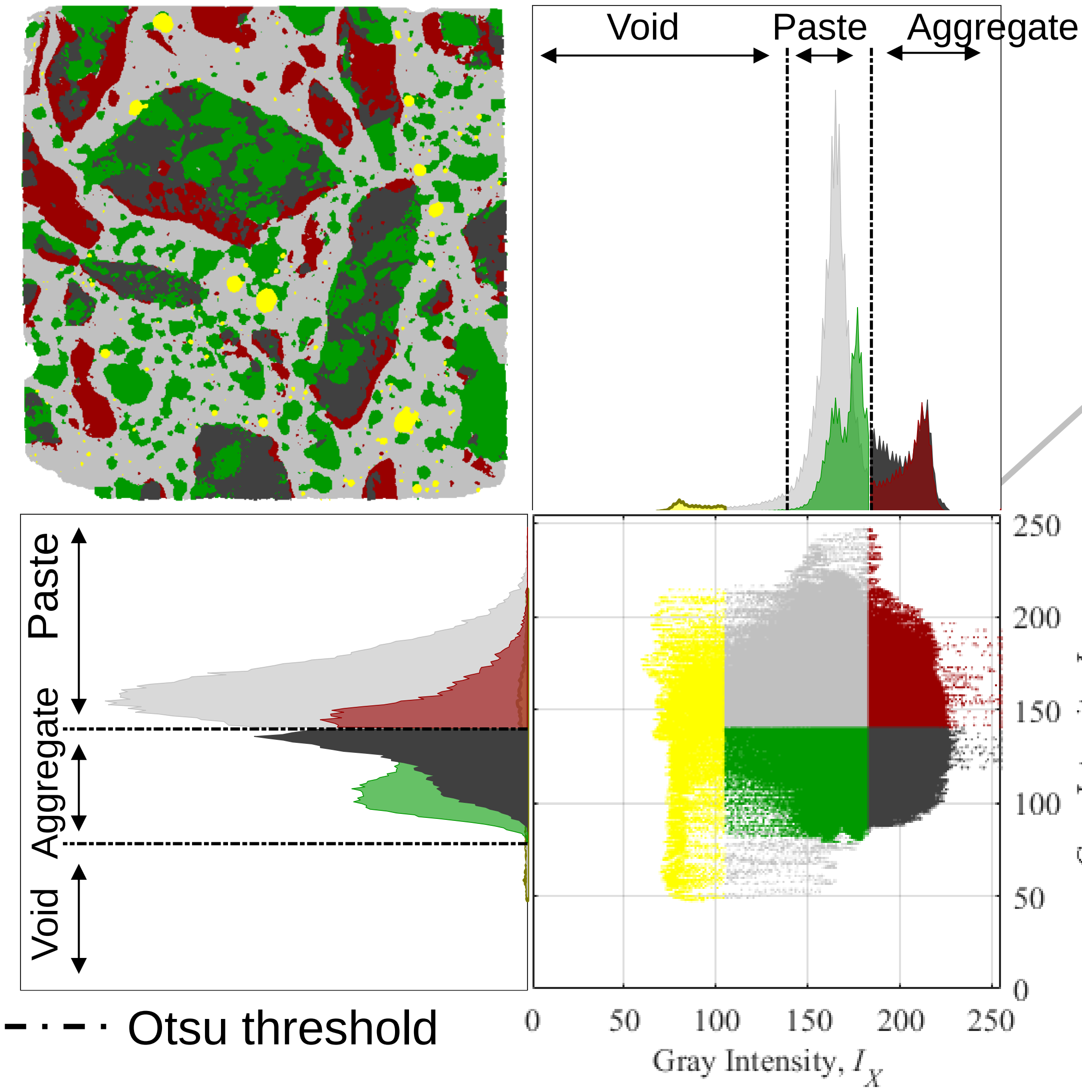

- Void
- Paste
- Aggregate (X-ray only)
- Aggregate (Neutron only)
- Aggregate (X-ray and neutron)

C-S-H (Paste)
$[(CaO)_3(SiO_2)_2(H_2O)_3 , \approx 2.60\ g/cm^2]$

Hornblend [각섬석](Gabbro)
$[(Ca, Na)_{2\sim3}(Mg, Fe, Al)_5(Al, Si)_8O_{22}(OH, F)_2 , \approx 3.31\ g/cm^2]$

Plagioclase [사장석] (Gabbro)
$[(Ca, Na)Al_2Si_2O_8 , \approx 2.67\ g/cm^2]$

Quartz [석영] (sand)
$[SiO_2 , \approx 2.65\ g/cm^2]$

Pyroxene [휘석] (Gabbro)
$[(Mg, Fe)_2Si_2O_6 , \approx 3.58\ g/cm^2]$

H.T. Kim, D.F.T. Razakamandimby, V. Szilagyi, K. Zoltan, L. Szentmiklosi, M.A. Glinicki, and K. Park, 2021 Reconstruction of concrete microstructure using complementarity of X-ray and neutron tomography, Cement and Concrete Research 148, 106540

Microstructure Reconstruction

◻ Aggregate Particle Size

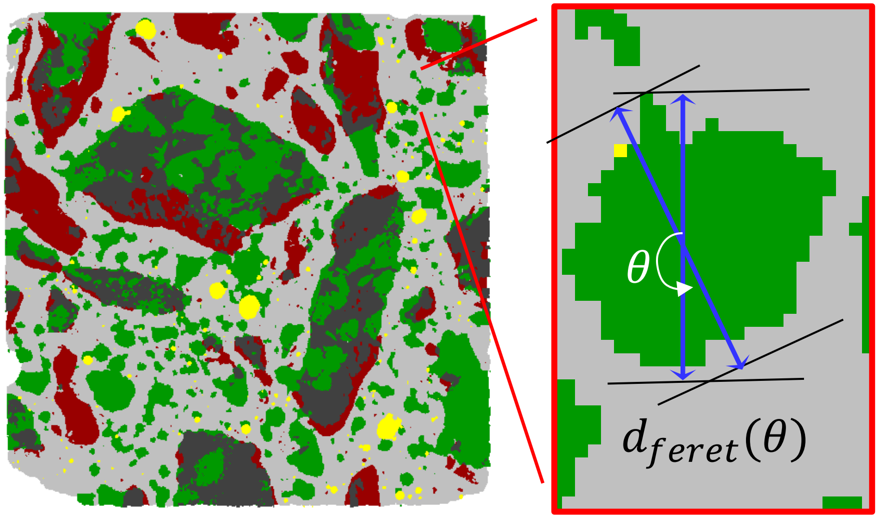

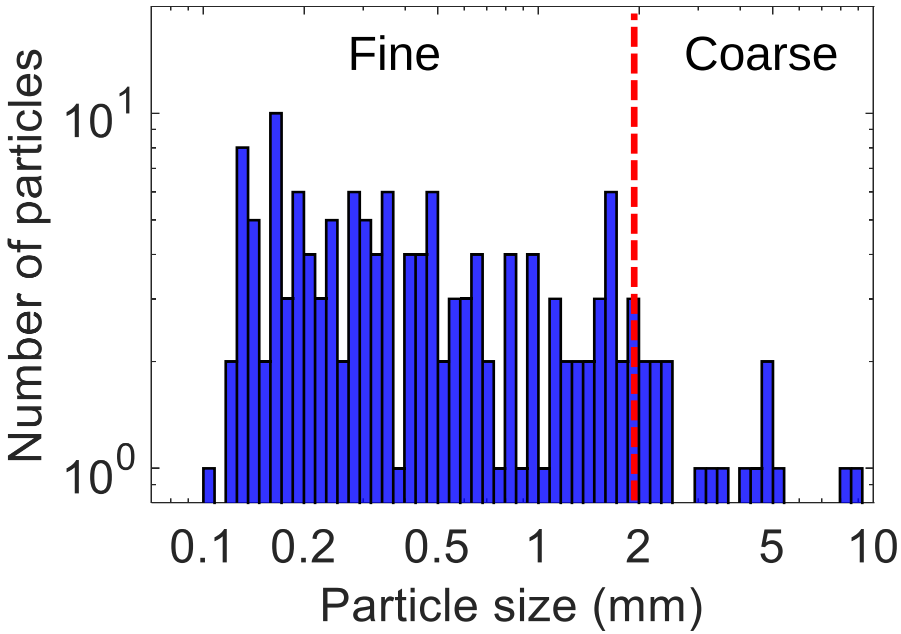

Particle size = $\frac{1}{180}\sum_{i=1}^{180} d_{feret}(\theta_i)$

Verification

◻ Microstructure

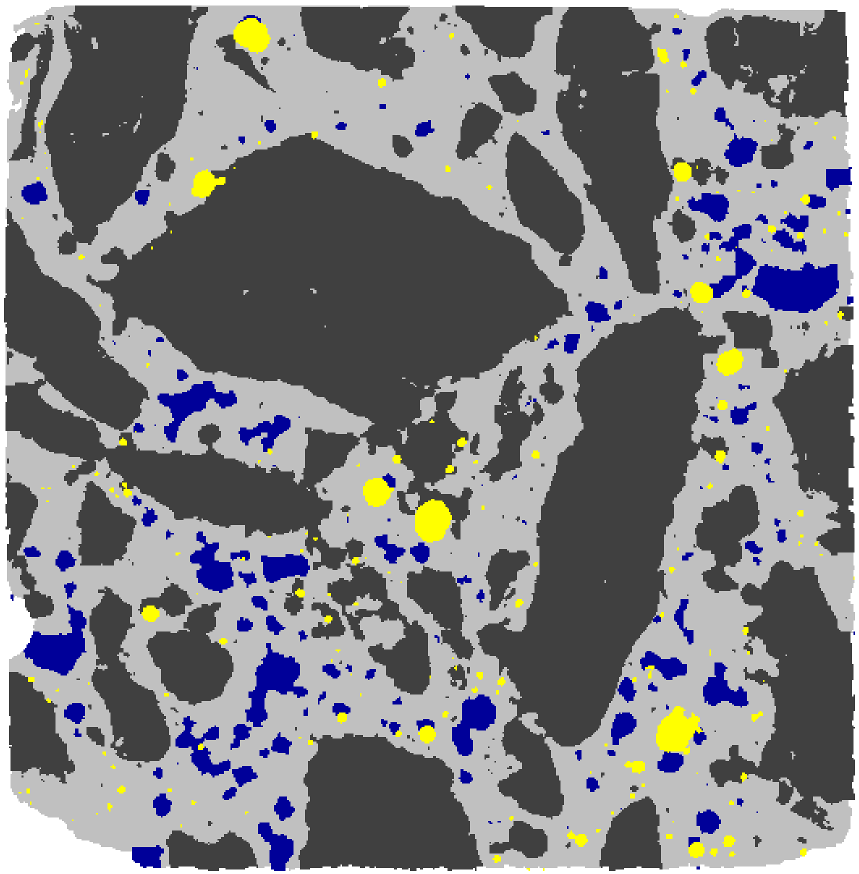

◻ Volume Fraction

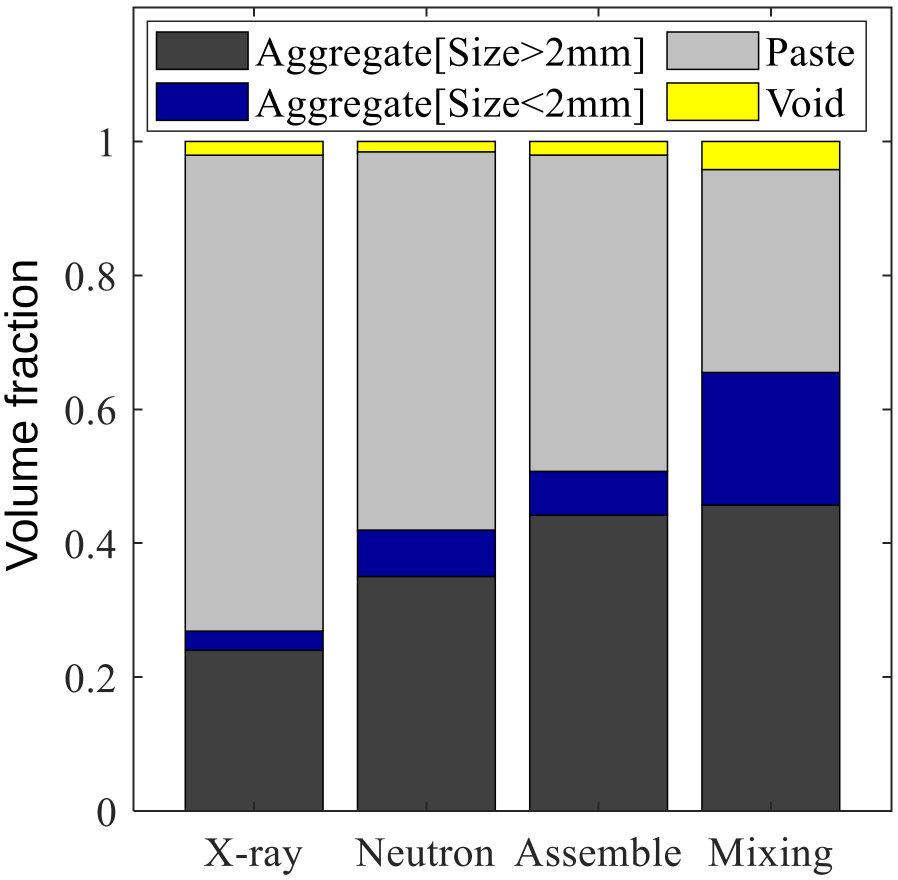

61 slides (10mm ~70mm)

Mesh Generation based on the Image

Microstructure

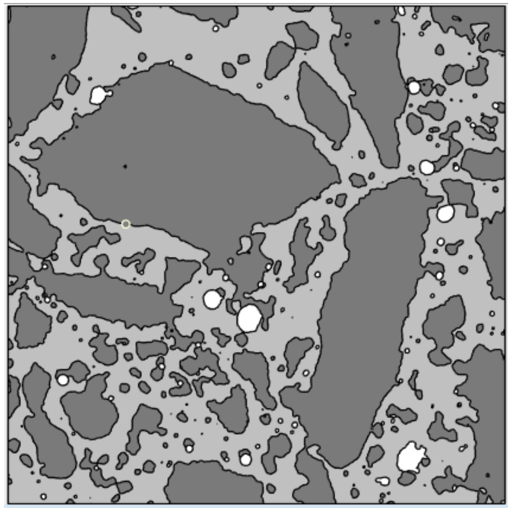

Centroidal Voronoi Tessellation (CVT)

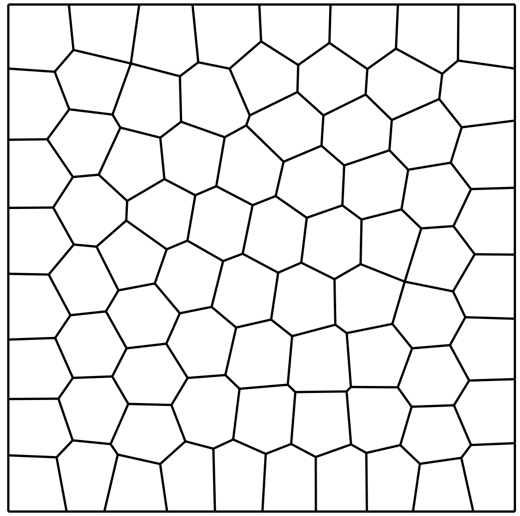

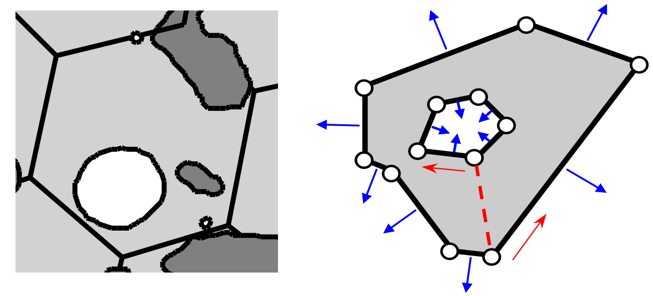

Non-simple Element

n_{elem} of CVT = 75

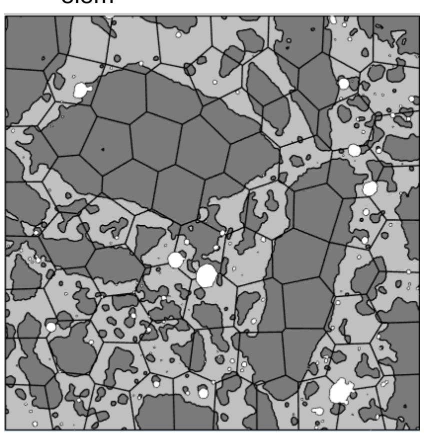

n_{elem} = 264

n_{elem} of CVT = 300

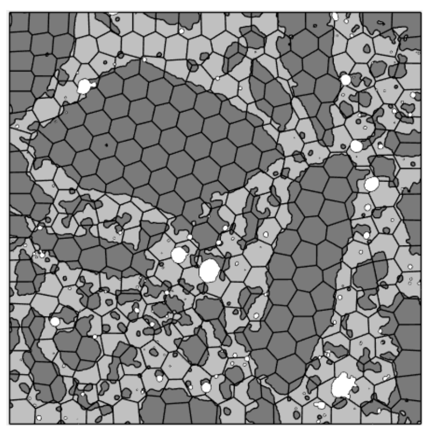

n_{elem} = 432

n_{elem} of CVT = 2500

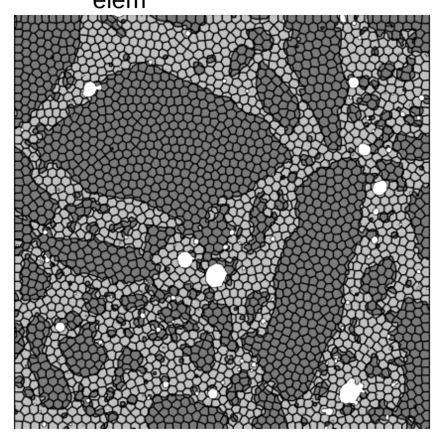

n_{elem} = 2497

n_{elem} of CVT = 10000

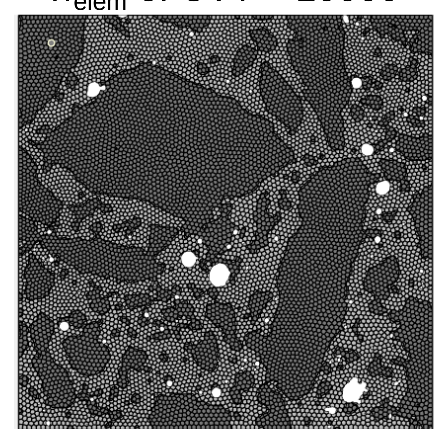

n_{elem} = 8956

Kim, H. T., & Park, K. 2022. Computed Tomography (CT) Image-based Analysis of Concrete Microstructure using Virtual Element Method. *Composite Structures*, 115937.

Virtual Element Formulation

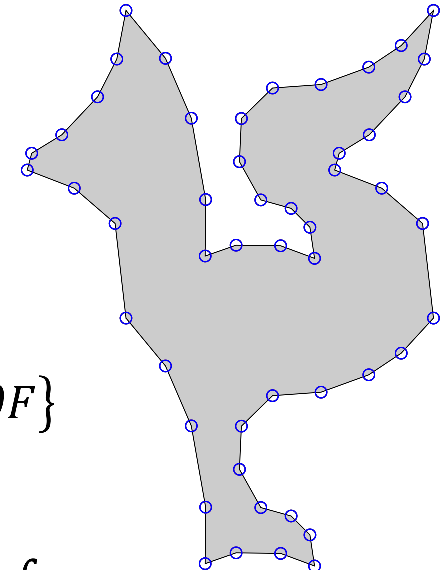

Governing Equation

$$\int_{\Omega} \boldsymbol{\epsilon}(\boldsymbol{u}) : \boldsymbol{\sigma}(\mathbf{v})\, d\mathbf{x} = \int_{\partial\Omega} \mathbf{v} \cdot \mathbf{t}\ d\mathbf{x} \quad \forall \mathbf{v} \in \mathcal{K}_0$$

Preliminary Space

$$\widetilde{\mathcal{V}}(F) = \{ v_h \in \mathcal{H}^1(F) : \Delta v_h \in \mathcal{P}_1(F) \text{ in } F, v_{h|e} \in \mathcal{P}_1(e)\ \forall e \in \partial F \}$$

First Projection by Projection Operator

$$\int_E \Pi^0 \nabla\phi_i \cdot \mathbf{m}_\alpha\, d\mathbf{x} = \sum S_{i\beta} \int_E \mathbf{m}_\beta \cdot \mathbf{m}_\alpha d\mathbf{x} = \int_{\partial E} \phi_i \mathbf{m}_i \cdot \mathbf{n}\, d\mathbf{s} - \int_E \phi_i \mathrm{div}\mathbf{m}_i d\mathbf{x}$$

Projection of Displacement

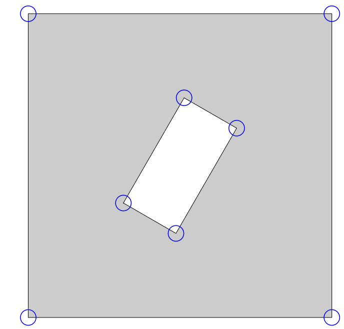

$$\int_E (\Pi^0 v_h) p\, d\mathbf{x} = \int_E v_h p\, d\mathbf{x} \quad \forall p \in \mathcal{P}(E)$$

$$p = \sum a_i \cdot m_i \quad m_1 = 1,\ m_2 = \left(\frac{x - x_c}{h_e}\right),\ m_3 = \left(\frac{y - y_c}{h_e}\right)$$

Beirão da Veiga, L., Brezzi, F., Cangiani, A., Manzini, G., Marini, L. D., & Russo, A, 2013, Basic principles of virtual element methods. *Mathematical Models and Methods in Applied Sciences*, 23(1), 199-214.

Uniaxial Tension Test

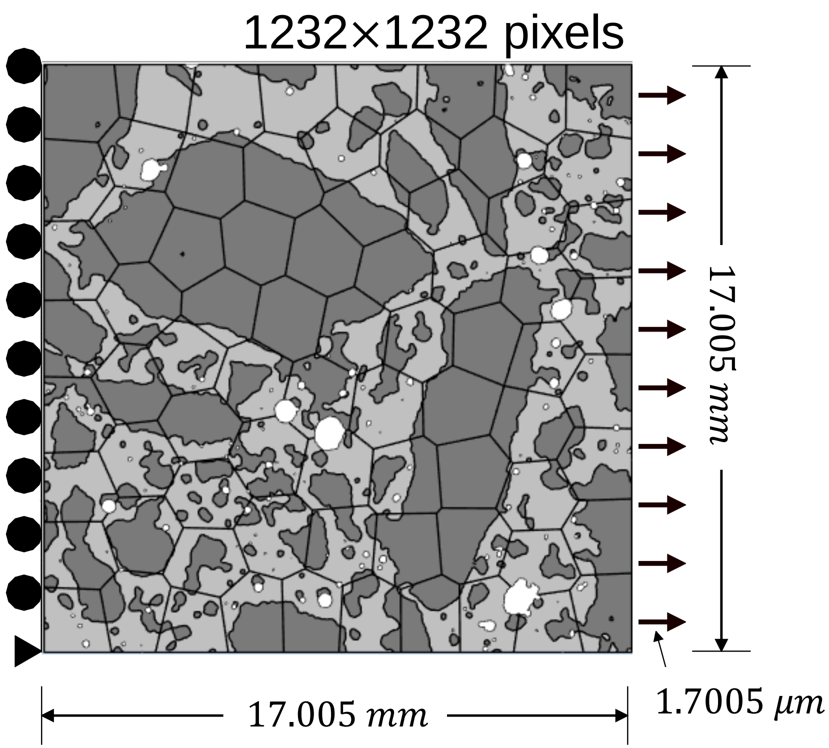

Meshes

- VEM mesh : 432, 632, 2,497, 4,812, and 9,021 elements
- n_{elem} in VEM meshes less than 0.604% of the Reference mesh

Reference solution

- Pixel-based FEM (Abaqus)
- $n_{elem} = 1{,}494{,}856$

Material Properties

- **Aggregate :** $E_a = 60$ GPa , $\nu_a = 0.25$
- **Paste :** $E_p = 20$ GPa , $\nu_p = 0.2$

Result

- Macro Elastic Modulus

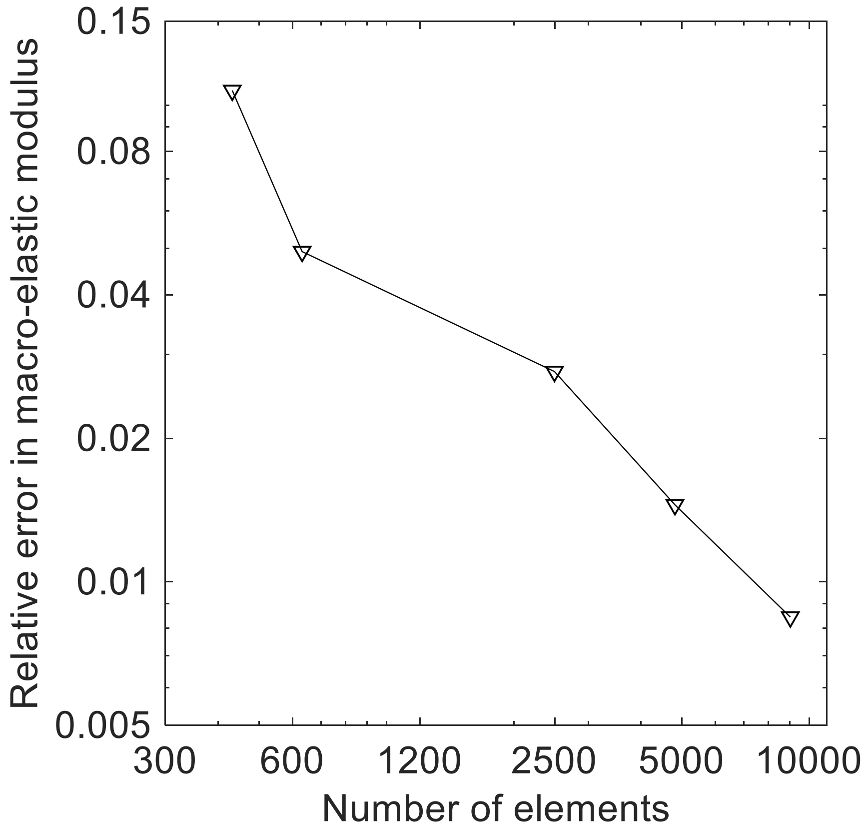

- Total Strain Energy

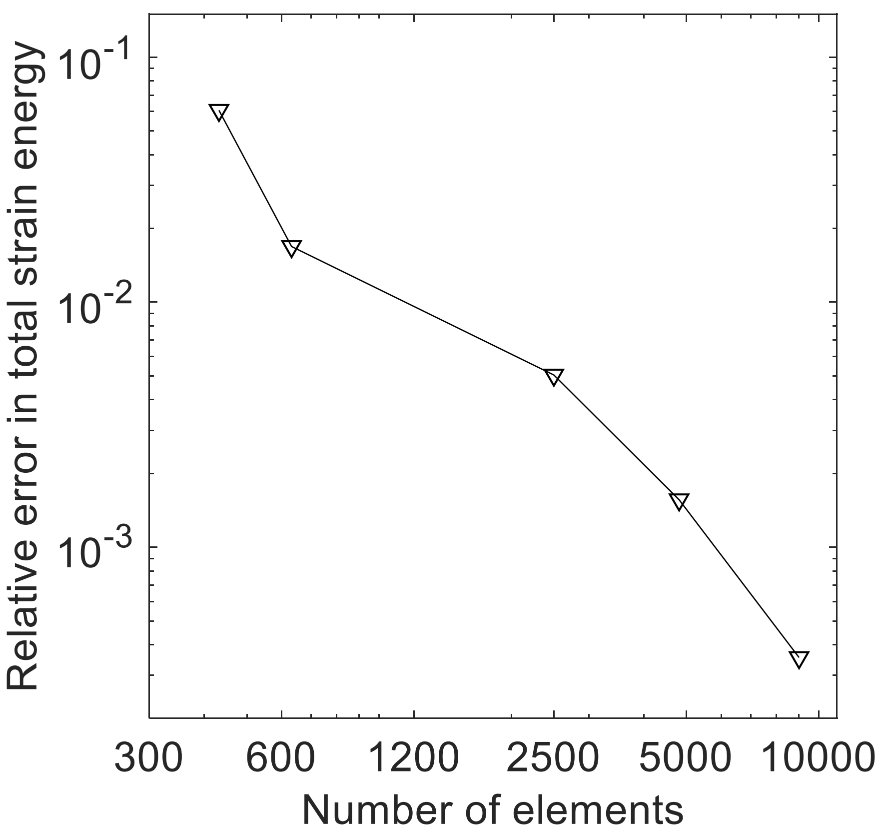

Aggregate Volume Expansion

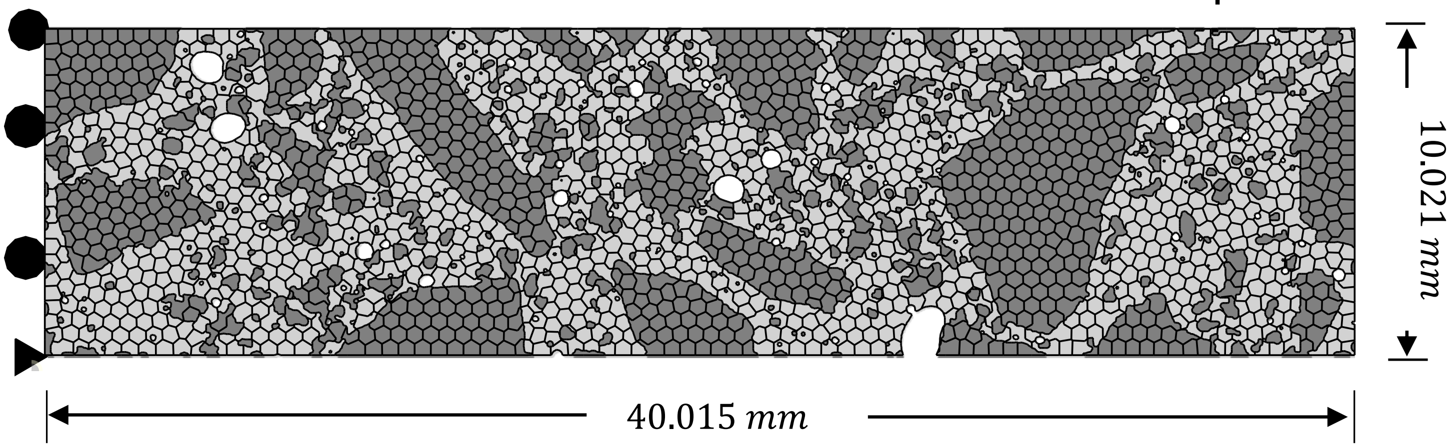

Material Properties

- **Aggregate**

$$\boldsymbol{E_a} = -3.16 \times 10^{-19} \boldsymbol{r_n} + 60.42 \qquad \nu_a = 0.25$$

$$\boldsymbol{\varepsilon_{V,a}} = 5.78 \left\{ 1 - \frac{1}{\sqrt{0.9997 + (1 - 0.9997)\exp[1.36 \times 10^{-15}(1 - 0.9997)\boldsymbol{r_n}]}} \right\}$$

- **Paste**

$$\boldsymbol{E_p} = -0.15 \times 10^{-19} \boldsymbol{r_n} + 22.25 \qquad \nu_p = 0.2$$

$$\boldsymbol{\varepsilon_{V,p}} = -3.1 \left\{ 1 - \frac{1}{\sqrt{0.9979 + (1 - 0.9979)\exp[2.588 \times 10^{-16}(1 - 0.9979)\boldsymbol{r_n}]}} \right\}$$

Jing, Y., & Xi, Y. (2017). Theoretical Modeling of the Effects of Neutron Irradiation on Properties of Concrete. *Journal of Engineering Mechanics*, *143*(12), 04017137. https://doi.org/10.1061/(asce)em.1943-7889.0001360

Irradiation Effect on the Material

Elastic modulus

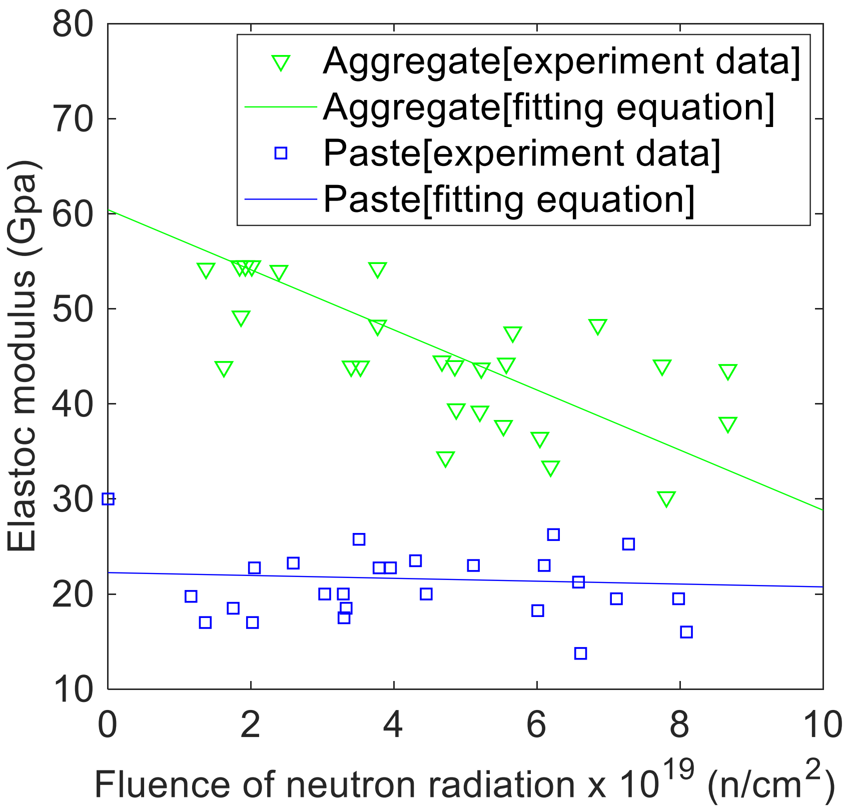

Volume change

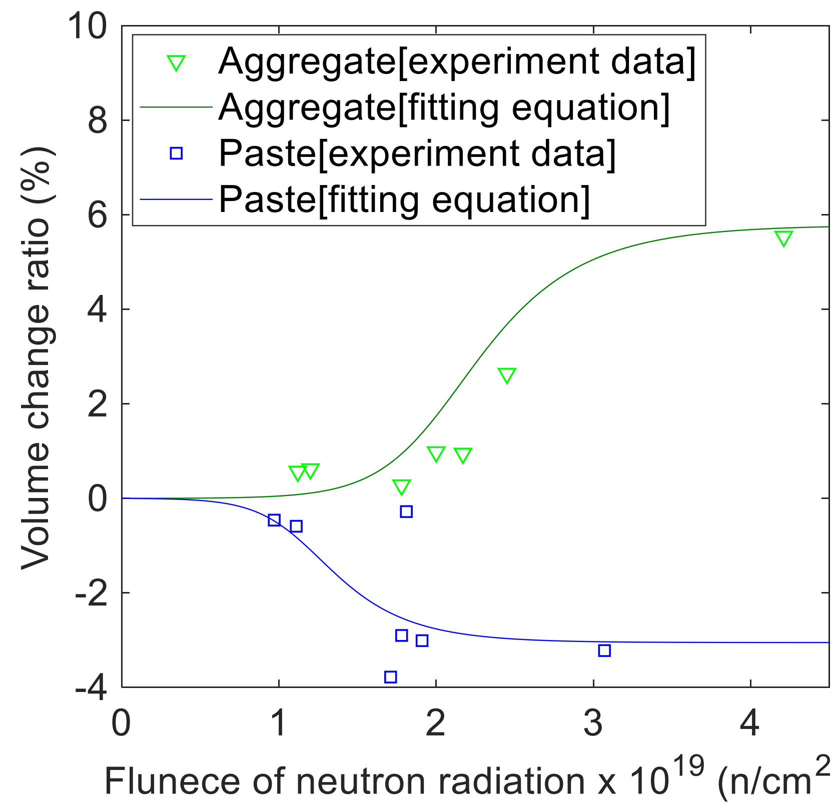

$$\boldsymbol{E} = a\boldsymbol{r_n} + b$$

$$\varepsilon_0 = \rho_{max}\left\{1 - \frac{1}{\sqrt{A + (1-A)\exp[B(1-A)\boldsymbol{r_n}]}}\right\}$$

Jing, Y., & Xi, Y. (2017). Theoretical modeling of the effects of neutron irradiation on properties of concrete. *Journal of Engineering Mechanics*, *143*(12), 04017137.

Result

◻ Volume Change

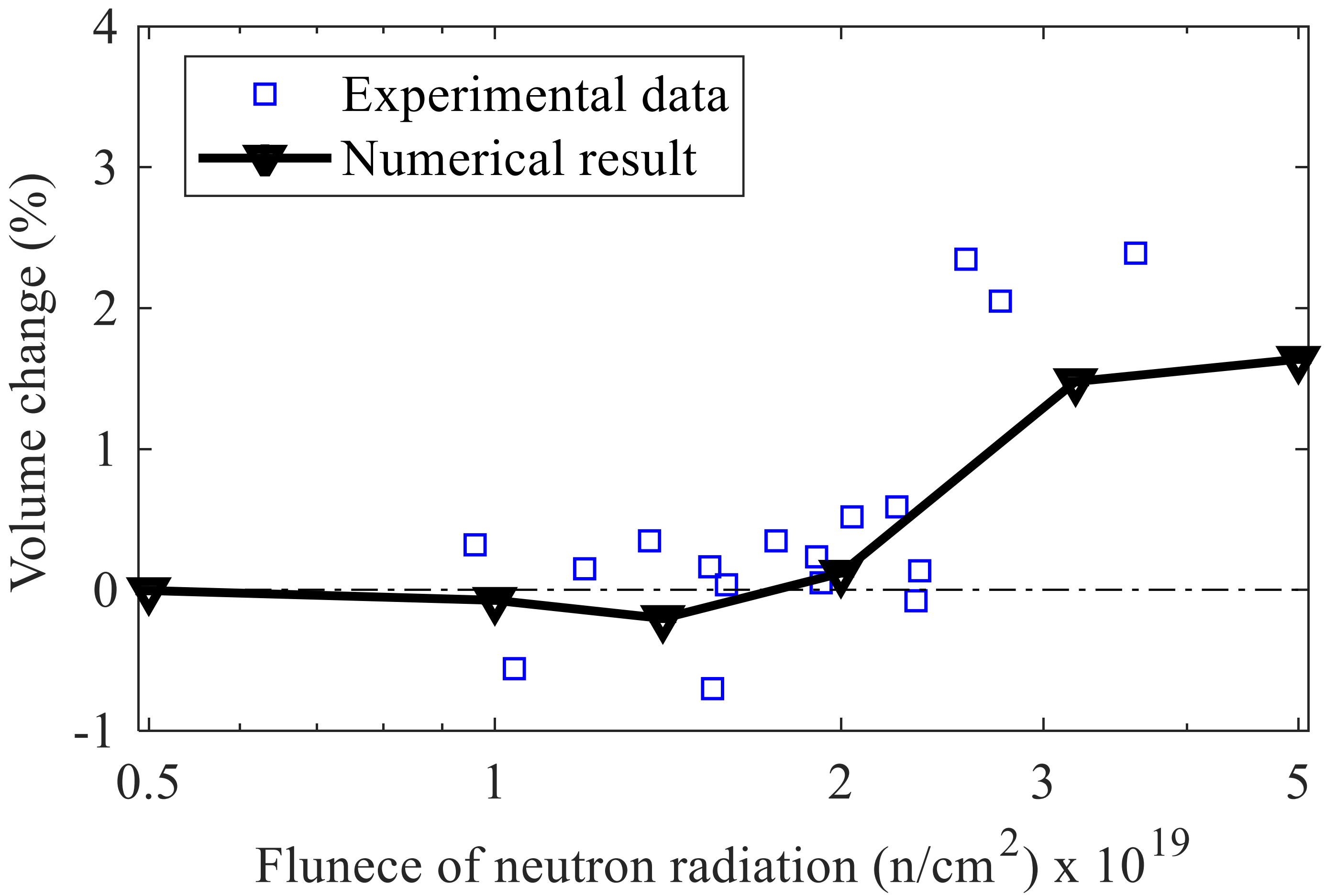

Elleuch, L. F., Dubois, F., & Rappeneau, J. (1972). Effects of neutron radiation on special concretes and their components. *ACI Special Publication*, *43*, 1071–1108.

Summary

- X-ray와 Neutron CT 를 상호보완하여 poly-mineral aggregate를 사용한 실제 콘크리트의 미세구조를 재구성한다.
- 재구성된 Digital image를 기반으로 다각형요소를 이용하여 복잡한 콘크리트 미세구조를 효율적으로 이산화 한다.
- 전체 요소개수에 상관없이 미세구조의 형상에 대한 정확성을 유지할 수 있으며, homogeneous mesh의 요소개수를 통해서 사용자가 요구하는 수치해석의 정확도를 확보한다.
- 이미지 기반 미세구조 해석을 통해 비파괴적 방법으로 중성자 조사환경과 같이 극한 환경에서 콘크리트의 재료특성 평가를 진행하고자 한다.

Question and Answer

Thank you

Irradiation effects on the Concrete

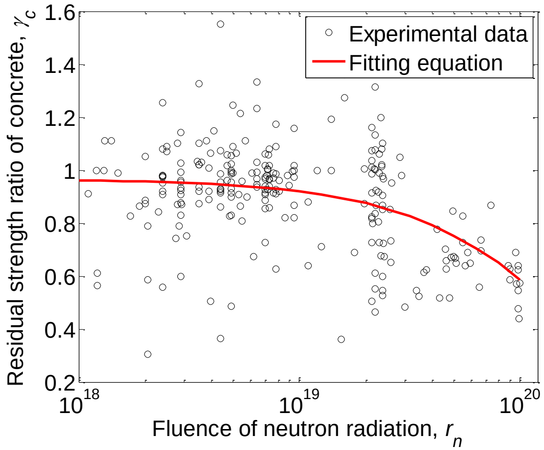

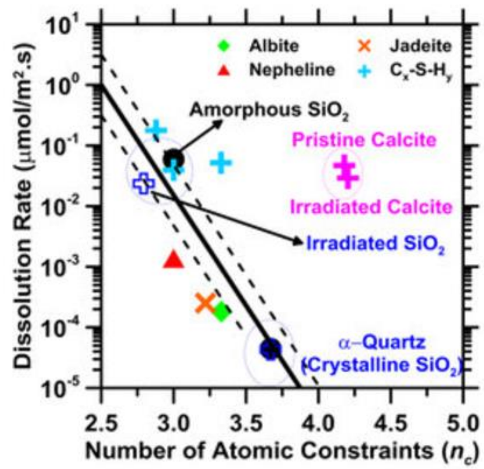

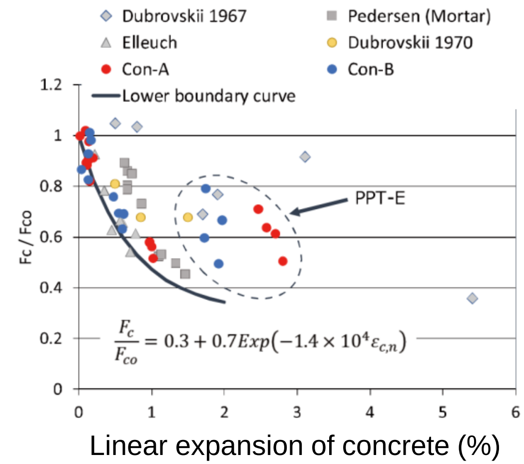

- Field, K. G., Remec, I., & Pape, Y. Le Pape., 2015. *Nuclear Engineering and Design*, 282, 126–143.
- K. Park, H.T. Kim, T.H. Kwon, and E. Choi, 2016, *Nuclear Engineering and Design* 310, 15-26
- Pignatelli, I., Kumar, A., Field, K.G., Wang, B., Yu, Y., Le Pape, Y., Bauchy, M. and Sant, G., 2016. *Scientific Reports*, 6, 20155
- Maruyama, I., Kontani, O., Takizawa, M., Sawada, S., Ishikawao, S., Yasukouchi, J., … Igari, T. 2017. *Journal of Advanced Concrete Technology*, 15(9), 440–523.

3D Concrete Microstructure

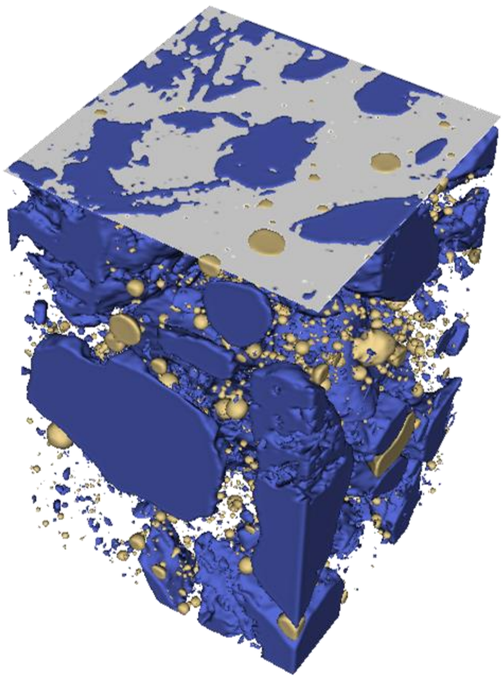

X-ray CT

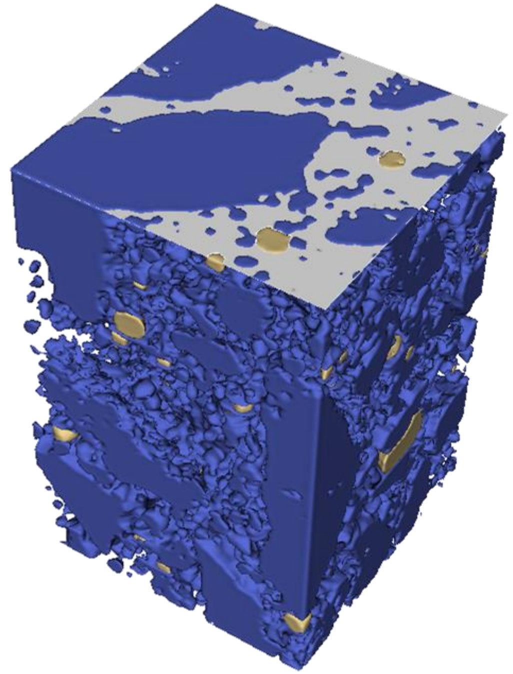

Neutron CT

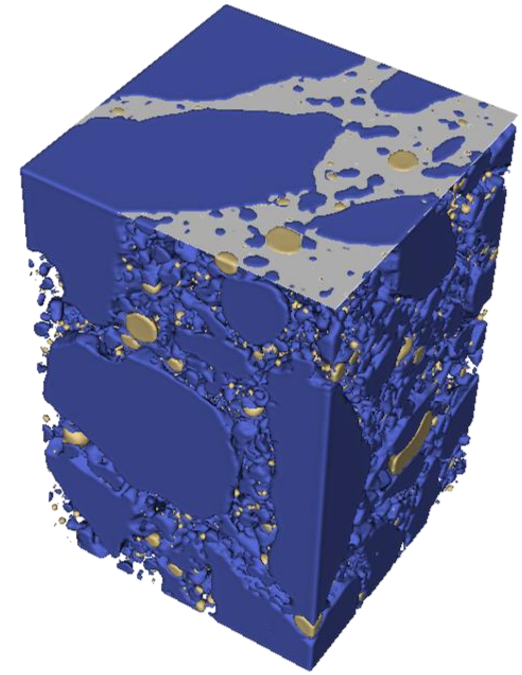

Assemble

H.T. Kim, D.F.T. Razakamandimby, V. Szilagyi, K. Zoltan, L. Szentmiklosi, M.A. Glinicki, and K. Park, 2021
Reconstruction of concrete microstructure using complementarity of X-ray and neutron tomography,
Cement and Concrete Research 148, 106540

Combined x-ray & neutron image

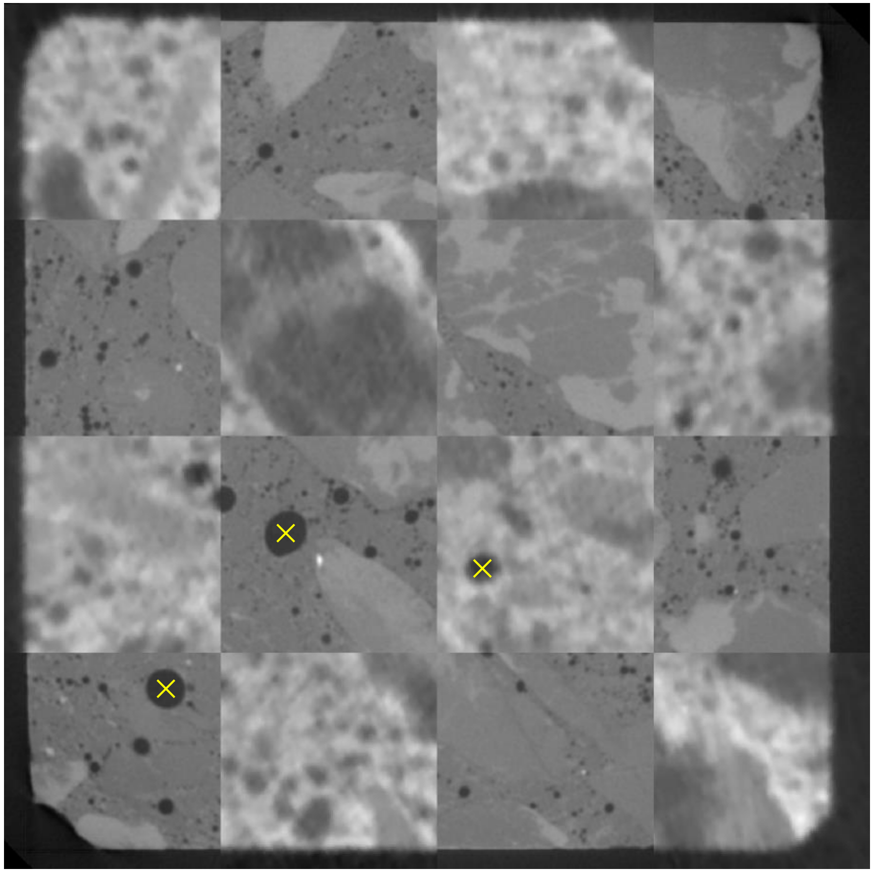

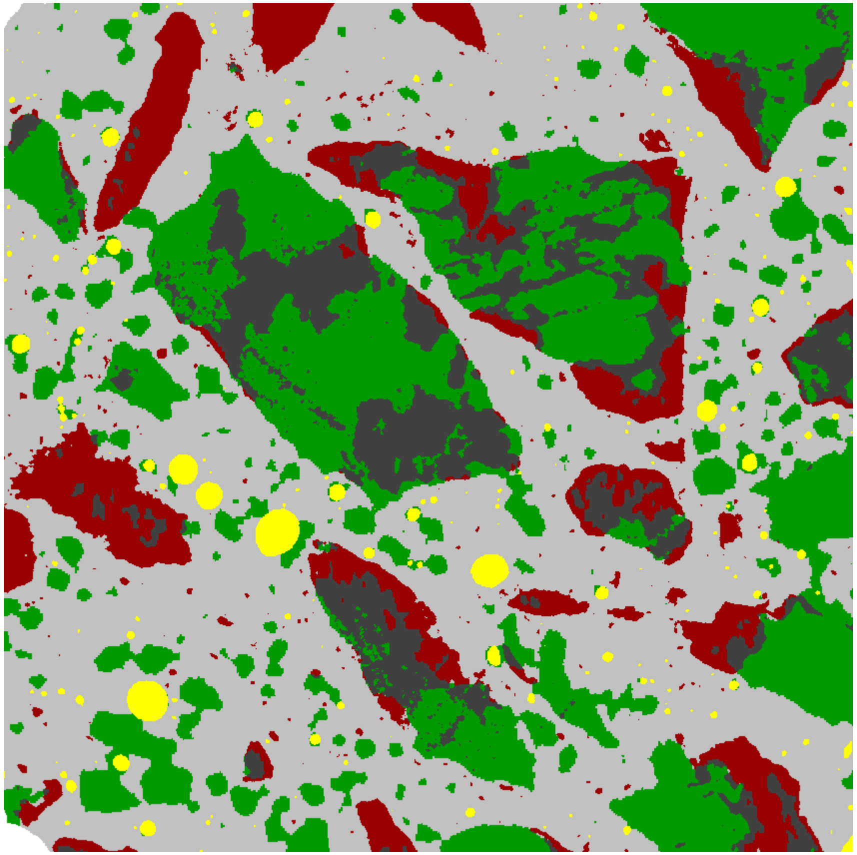

Morphological Filtering

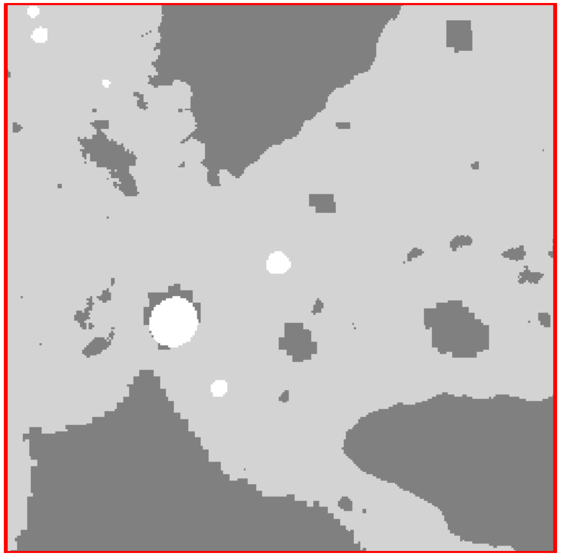

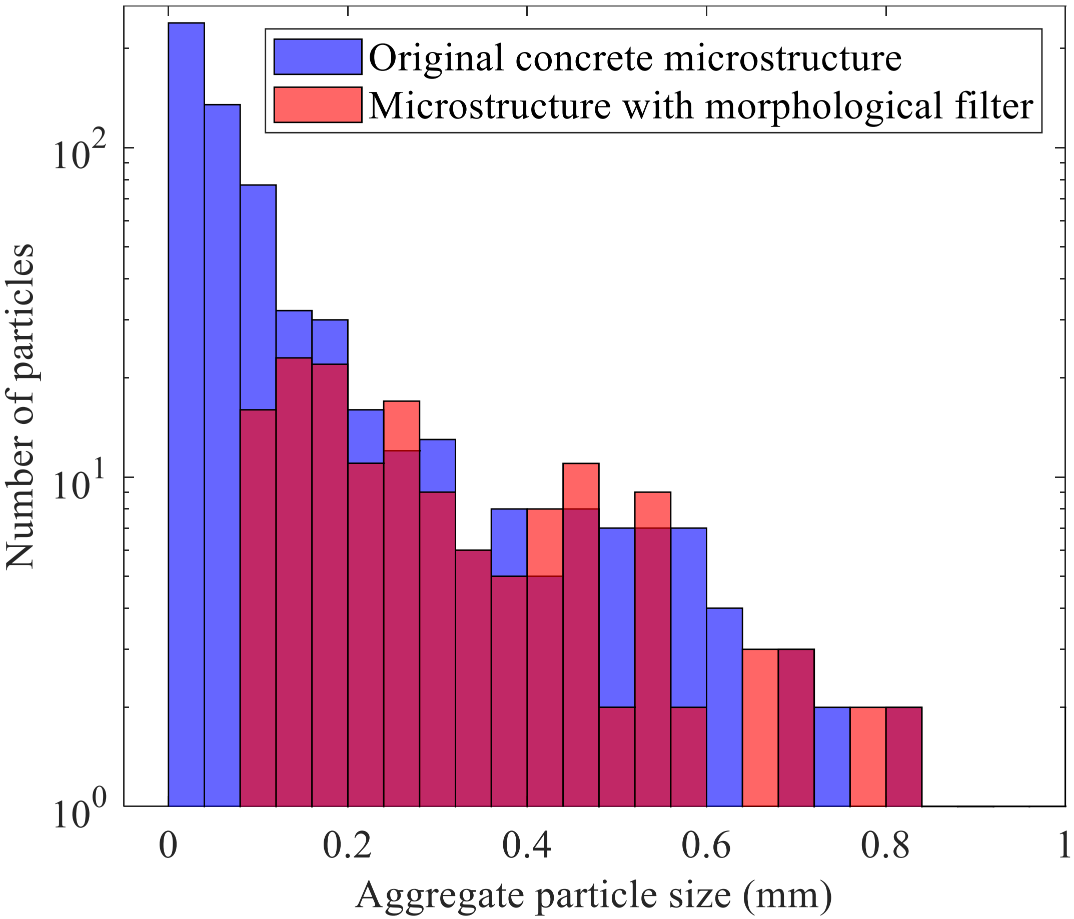

Mesh Generation

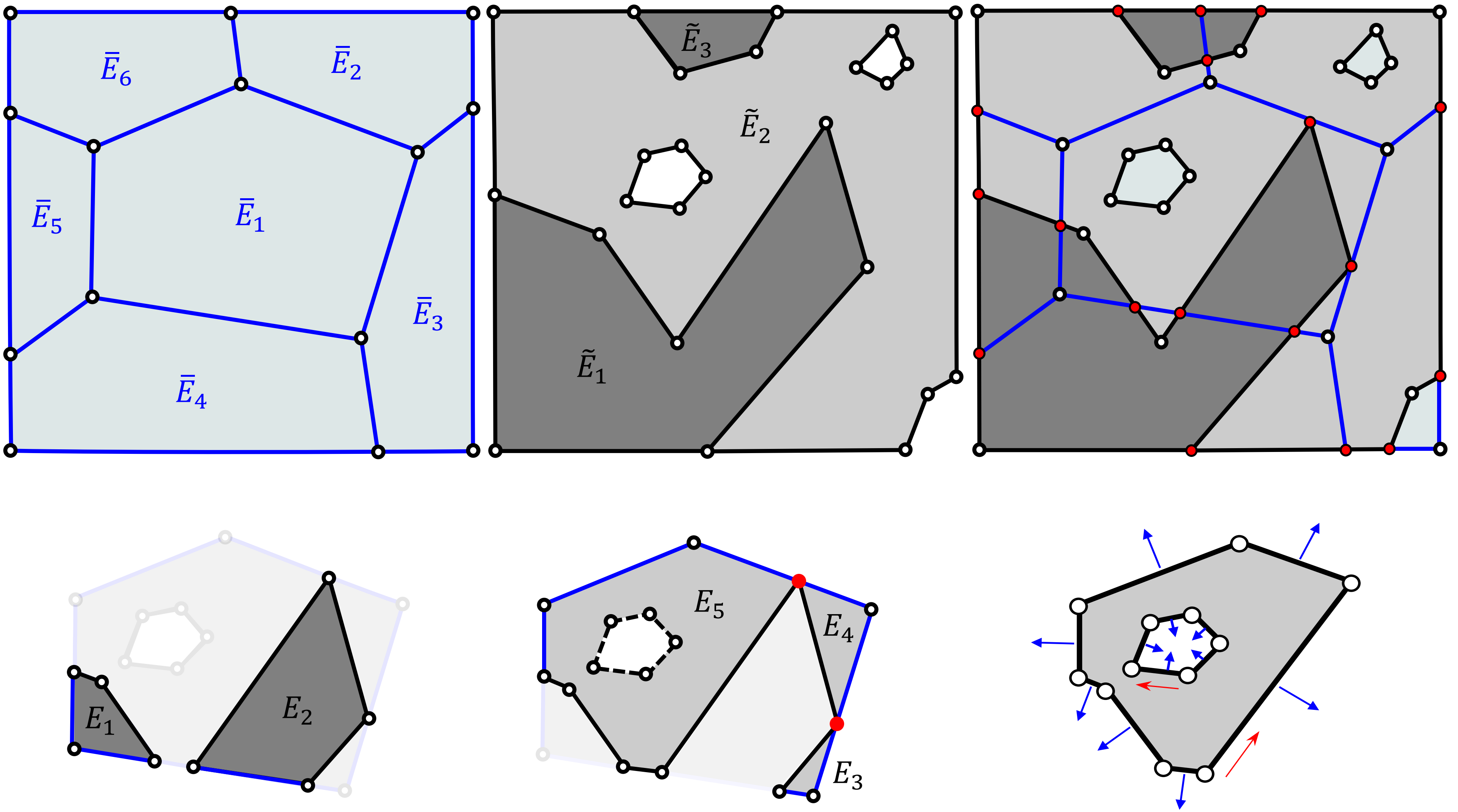

Non-simply connected elements

L^2 Projection Operator

Projection of Displacement

$$\int_E (\Pi_1^0 v_h) p_1 \, d\mathbf{x} = \int_E v_h p_1 \, d\mathbf{x} \quad \forall p_1 \in \mathcal{P}_1(E)$$

$$p_1 = \sum_{\alpha=1}^{n_{p_1}} \alpha_\alpha m_\alpha \qquad m_1 = 1,\ m_2 = \frac{x - x_c}{h_P},\ m_3 = \frac{y - y_c}{h_P},\ m_4 = \frac{z - z_c}{h_P}$$

Projection of Strain

$$\int_E (\Pi_0^0 \nabla v_h) \cdot \mathbf{p}_0 \, d\mathbf{x} = \int_E \nabla v_h \cdot \mathbf{p}_0 \, d\mathbf{x} \quad \forall \mathbf{p}_0 \in [\mathcal{P}_0(E)]^2$$

$$\mathbf{p}_0 = \sum_{\alpha=1}^{n_{\mathbf{p}_0}} a_\alpha \mathbf{m}_\alpha \qquad \mathbf{m}_1 = \begin{bmatrix} 1 \\ 0 \\ 0 \end{bmatrix}, \mathbf{m}_2 = \begin{bmatrix} 0 \\ 1 \\ 0 \end{bmatrix}, \mathbf{m}_3 = \begin{bmatrix} 0 \\ 0 \\ 1 \end{bmatrix}$$

$$\int_E \Pi_0^0 (\nabla v_h) \cdot \mathbf{p}_0 \, d\mathbf{x} = \int_{\partial E} v_h \mathbf{p}_0 \, d\mathbf{x} - \int_E v_h \mathrm{div}(\mathbf{p}_0) \, d\mathbf{x}$$

Construction of Stiffness Matrix

◻ Element Stiffness Matrix

$$\mathbf{K}_E = \mathbf{K}_{E,c} + \mathbf{K}_{E,s}$$

$$\mathbf{K}_{E,c} = \int_E \mathbf{B}^T \mathbf{C} \mathbf{B} \, d\mathbf{x}$$

$$\mathbf{B} = \sum_{\alpha=1}^{d} [\Pi_0^0 \nabla \boldsymbol{\phi}]_\alpha \otimes \overline{\mathbf{B}}_\alpha$$

$$\overline{\mathbf{B}}_1 = \begin{bmatrix} 1 & 0 \\ 0 & 0 \\ 0 & 1 \end{bmatrix}, \quad \overline{\mathbf{B}}_2 = \begin{bmatrix} 0 & 0 \\ 0 & 1 \\ 1 & 0 \end{bmatrix} \quad \text{for 2D}$$

$$\overline{\mathbf{B}}_1 = \begin{bmatrix} 1 & 0 & 0 \\ 0 & 0 & 0 \\ 0 & 0 & 0 \\ 0 & 1 & 0 \\ 0 & 0 & 0 \\ 0 & 0 & 1 \end{bmatrix}, \quad \overline{\mathbf{B}}_2 = \begin{bmatrix} 0 & 0 & 0 \\ 0 & 1 & 0 \\ 0 & 0 & 0 \\ 1 & 0 & 0 \\ 0 & 0 & 1 \\ 0 & 0 & 0 \end{bmatrix}, \quad \overline{\mathbf{B}}_3 = \begin{bmatrix} 0 & 0 & 0 \\ 0 & 0 & 0 \\ 0 & 0 & 1 \\ 0 & 0 & 0 \\ 0 & 1 & 0 \\ 1 & 0 & 0 \end{bmatrix} \quad \text{for 3D}$$

$$\mathbf{K}_{E,s} = \overline{\mathbf{K}}_{E,s} \otimes \mathbf{I}_d$$

$$\overline{\mathbf{K}}_{E,s} = (\mathbf{I}_n - \mathbf{P}_1^0)^T \boldsymbol{\Lambda} (\mathbf{I}_n - \mathbf{P}_1^0)$$

K. Park, H. Chi, and G.H. Paulino, 2020, Numerical recipes on virtual element method for elasto-dynamic explicit time integration, International Journal for Numerical Methods in Engineering 121, 1-31

Mesh Generation based on the Image

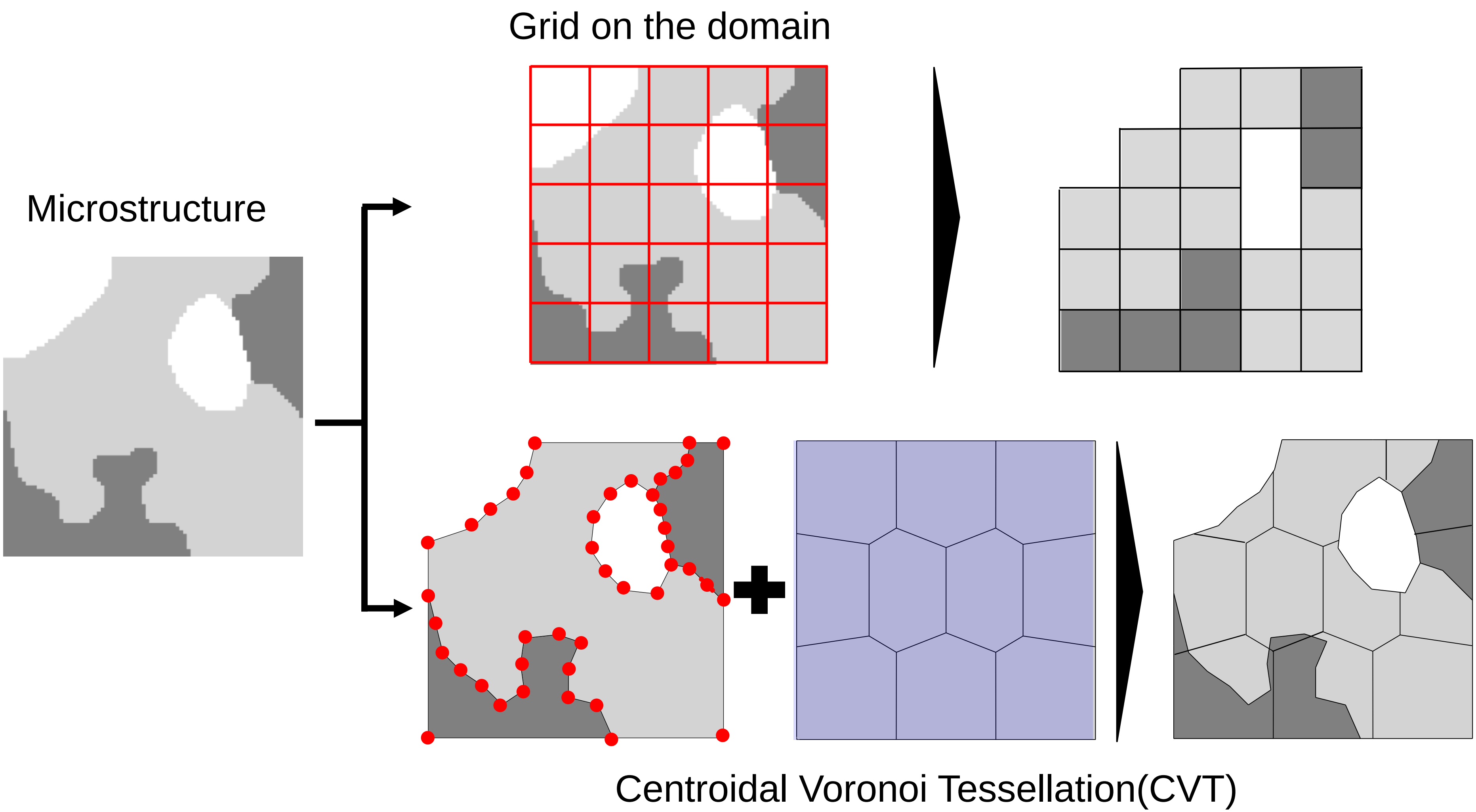

Kim, H. T., & Park, K. 2022. Computed Tomography (CT) Image-based Analysis of Concrete Microstructure using Virtual Element Method. *Composite Structures*, 115937.

VEM vs FEM

◻ Macro Elastic Modulus

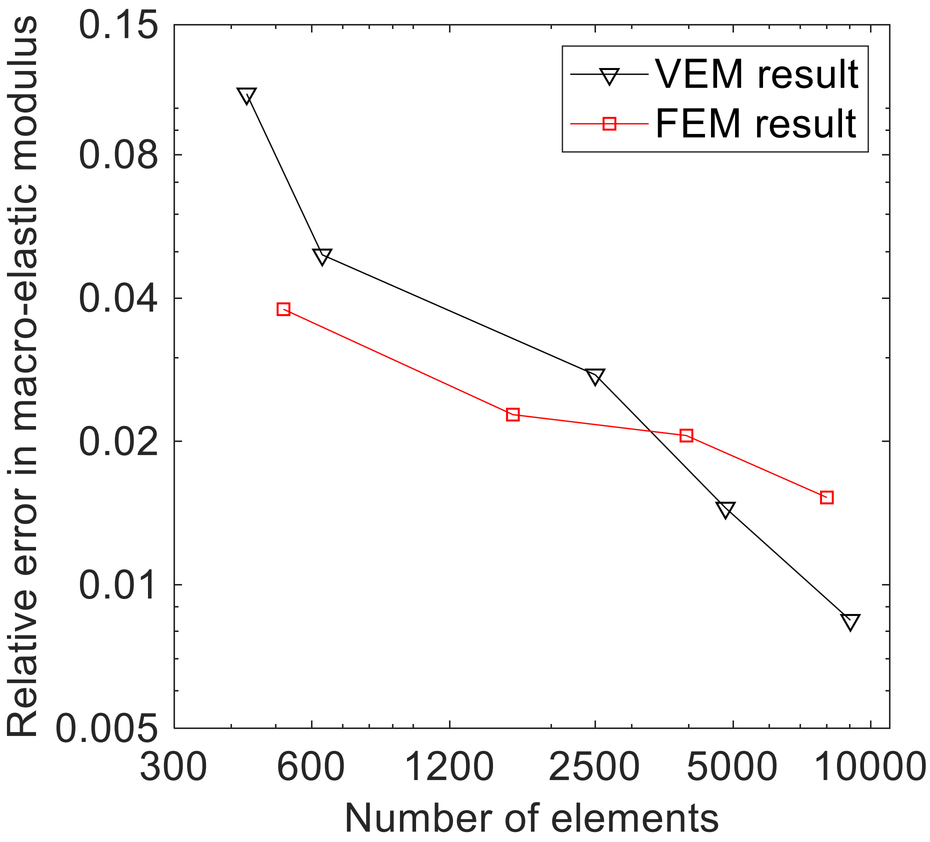

◻ Total Strain Energy

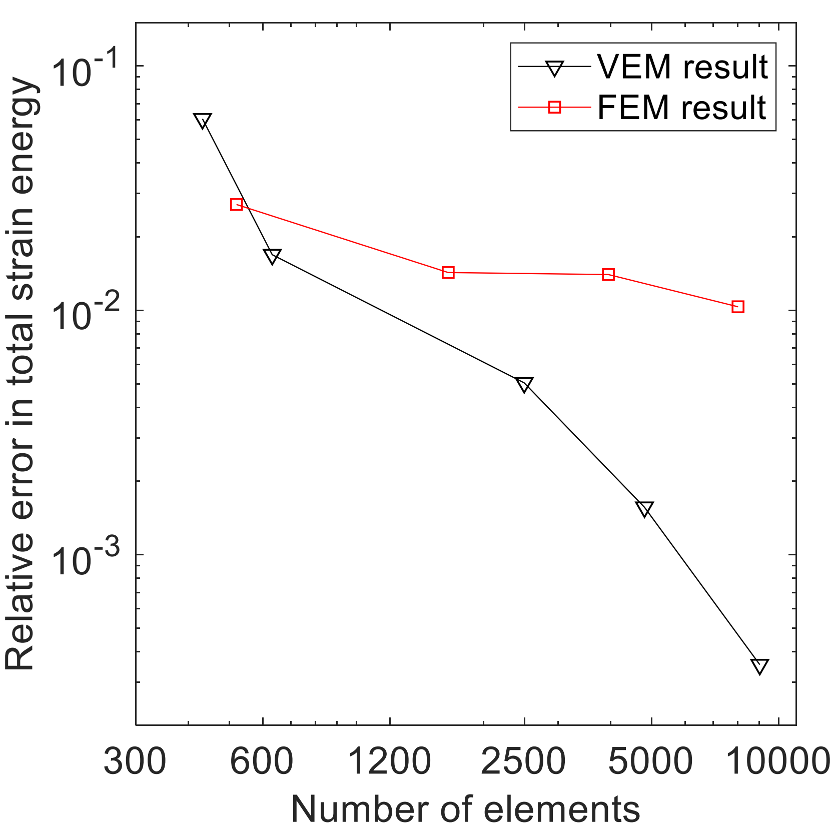

Hyeongtae Kim (shape1729@yonsei.ac.kr)
Computational & Experimental Mechanics Group

Meshes

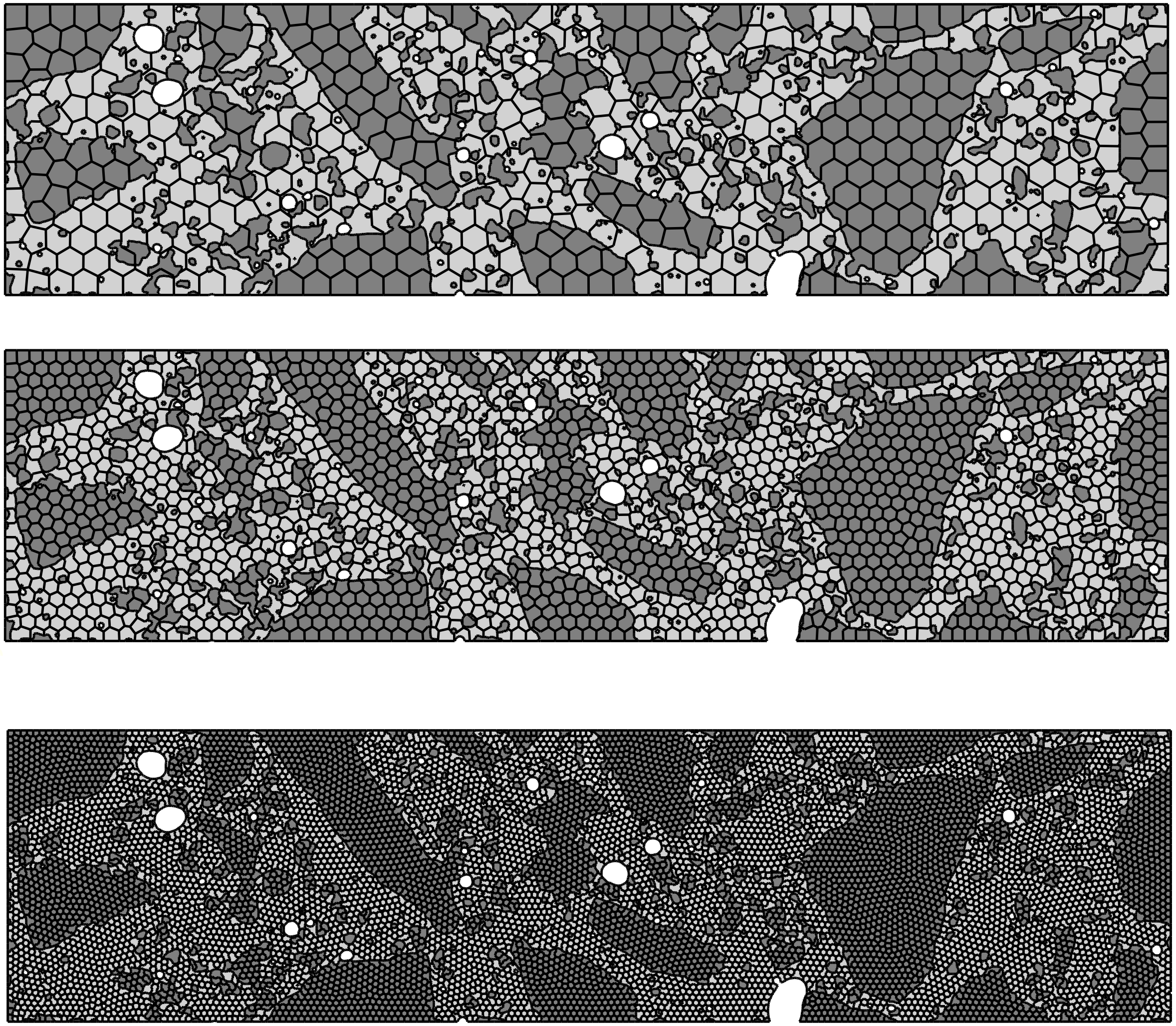

Aggregate Volume Expansion

◻ Horizontal stress field

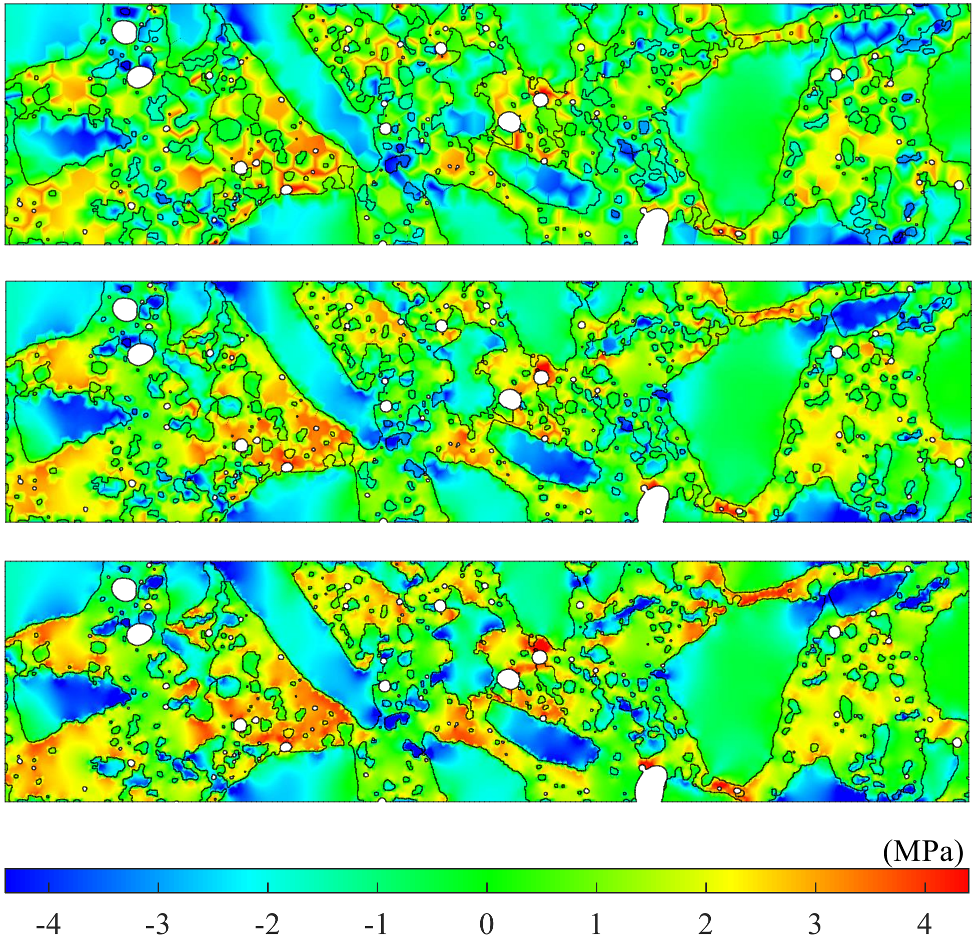

Aggregate Volume Expansion

- **Strain error :** H^1**-type skeletal norm error**